On the Use of Transfer Approaches to Predict the Vibroacoustic Response of Poroelastic Media

Quentin Serra, Mohamed Ichchou, Jean-François Deü

On the Use of Transfer Approaches to Predict the Vibroacoustic Response of Poroelastic Media

Q. Serra[†]
Université d'Orléans, Laboratoire PRISME, Orléans, France
quentin.serra@ec-lyon.fr

M. N. Ichchou[‡]
[*]*École Centrale de Lyon*
Laboratoire de Tribologie et de Dynamique des Sysèmes
Écully 69130, France
mohamed.ichchou@ec-lyon.fr

J.-F. Deü
[†]*Conservatoire National des Arts et Métiers*
Laboratoire des Mécanique des Structures et des Systèmes Couplés
Paris 75003, France
jean-francois.deu@cnam.fr

The transfer matrix method (TMM) is a famous analytic method in the vibroacoustic community. It is classically considered as a high frequency approach, because of the hypothesis of acoustic plane waves impinging on a flat infinite panel. Thus, it cannot take into account directly finite-size effects or lateral boundary conditions (BCs), and it needs specific algorithms to correct its results in the low frequency range. Within the transfer matrix framework, the use of finite elements makes it possible to generalize the range of applications of transfer approaches. Thus, the study of wave propagation in poroelastic media, in presence of lateral BCs can be carried out. The links between theses waves and the acoustic response of a sample are investigated. Finally, it shows that transfer approaches are not limited in the low frequency range, as usually stated. In fact, the validity of analytic transfer approaches depends more on the material and on the geometry than on the frequency range.

Keywords: Wave propagation; waveguide with lateral boundary conditions; numerical and analytical transfer approaches; transfer matrix method; wave finite element method.

1. Introduction

Transfer approaches have been extensively used in the literature since first works from Thomson and Haskell.[1,2] They are used in various scientific domains, from electromagnetism, quantum mechanics, to solid mechanics and seismic wave propagation, because they are particularly well fitted to deal with wave propagation problems.

Among this class of methods, the so-called transfer matrix method (TMM)[3,4] is a global transfer matrix approach dedicated to the prediction of the vibroacoustic response of the dissipative layers used in transport industry, for either acoustic absorption or transmission problems. Such interfaces are typically composed of poroelastic layers. These materials are composed of a skeleton perforated by a network of interconnected pores. They are thus very light and are able to dissipate very efficiently acoustic waves traveling inside their pores.

The response of such materials can also be predicted by using the finite element method (see, e.g. Refs. 5 and 6). However, it leads to an expensive computational cost. Indeed, poroelastic materials may be of small thickness, they exhibit very small wavelengths. In the general case, one needs to consider both the solid phase and the fluid phase, leading to a very large number of degrees of freedom to solve. Furthermore, material parameters are frequency dependent, resulting in expensive computations when a large frequency band is considered. To tackle this problem, an idea consists in the use of hybrid finite element — wave based models, where the porous domain, which is the expensive part, is modeled analytically. Among such models can be found the FEM-TMM[7,8] or the WBM-TMM.[9]

Waves are propagating in the entire frequency range, covering from the vibroacoustic way of thinking low, medium and high frequencies. Thus, transfer approaches should be valid in the entire frequency range. On the contrary, TMM is usually presented as a high frequency approach. When the wavelengths are short with respect to the geometry, the medium can be considered as flat and infinite, and the TMM may be used. In the low frequency range, some corrections have been proposed to correct finite size effects by using spatial windowing techniques.[3,10,11] However, the low frequency correction consists only in a finite size correction, so it does not really take into account the effects of lateral boundary conditions (BCs), typically when the sample is sliding or clamped on its lateral faces.

These observations lead to a contradiction: In one hand, transfer matrix formalism applies in the entire frequency range, while on the other hand, the TMM seems to be only pertinent in the high frequency range, where the lateral BC and finite-size effects can be neglected. The aim of this work is thus to discuss the foundation of the TMM, to show how transfer approaches can be used to predict the vibroacoustic response of materials and to analyze it on wave insights.

The present paper is structured as follows. In a first part, the state space form of the system of the equations resulting from the mechanics of continuous media is briefly recalled. This formalism consists in an exact reformulation of the dynamic equilibrium of the medium, making it possible to express a transfer operator traducing how waves travel in the medium. This shows that wave approaches should not depend on frequency nor BCs.

Then, several transfer approaches are reviewed. It is observed that TMM derives exactly from the analytic approach, with the only assumption of plane wave propagation in the material. Finite elements can be used in the transfer matrix framework, resulting in a method called Wave Finite Element (WFE) Method.[12,13] Using finite elements allows both lateral BCs and finite size effects to be taken into account, this method can thus be considered as an extension of the TMM. In Sec. 3, the influence of BCs is investigated for three different materials covering for the large range of poroelastic materials used in vibroacoustics, in the case of an uniform pressure field, and for two BCs: Sliding BC and clamped BC. These BCs are representative of what can happen in an impedance tube. The effect of such BCs on the vibroacoustic response has been thoroughly investigated in previous papers, both experimentally or numerically (see, e.g. Refs. 14–16), we propose here a novel analysis based on the observation of the properties of the waves traveling inside the material. This study is followed by two cases of nonuniform loading, making it possible to observe some limits of the analytical approaches, both in the low or the high frequency range. Finally, Sec. 5 concludes the paper.

2. Transfer Approaches in a Medium

2.1. *State space approach of a medium: Stroh's formalism*

We consider first a three-dimensional homogeneous linear elastic medium, parameterized in Cartesian coordinates (x, y, z). The thickness of the panel is oriented in z direction, while the sections are parallel to the plane (x, y). In frequency domain and without body loads, the dynamic equilibrium is classically written:

$$\boldsymbol{\nabla} \cdot \boldsymbol{\sigma} = -\rho\omega^2 \mathbf{u}, \tag{1a}$$

$$\boldsymbol{\sigma} = \frac{1}{2}\mathbf{C} : (\boldsymbol{\nabla}\mathbf{u} + \boldsymbol{\nabla}^T\mathbf{u}), \tag{1b}$$

where $\boldsymbol{\sigma}$ is the stress tensor, $\mathbf{u} = (u_x, u_y, u_z)^T$ the displacement, ρ the density, ω the angular frequency and $\mathbf{C}$ the tensor of the elasticity constants. Such writing can be called dynamic stiffness formulation, because the load vector $\boldsymbol{\nabla} \cdot \boldsymbol{\sigma}$ is expressed as a function of the displacement $\mathbf{u}$.

For poroelastic media, several formulations exist: Either equivalent fluid models, classically limp and rigid frame limits, or the Biot–Allard model with the choice of the variables (displacement–displacement,[17] displacement–pressure,[5,18] or displacement–total displacement[19]). It is well-known that all of these models are equivalent in frequency domain for materials which can be modeled with Johnson–Champoux–Allard's coefficients. In this work, the displacement–total displacement $(\mathbf{u}^s, \mathbf{u}^t)$ formulation has been used, the corresponding equations of the dynamic equilibrium are given in Appendix B.

In the state space, the dynamic equilibrium can be rewritten as:

$$\mathbf{J}\frac{\partial}{\partial z}\mathbf{V}(\omega, x, y, z) = \mathbf{H}(\omega)\mathbf{V}(\omega, x, y, z), \tag{2}$$

where $\mathbf{J}$ is the symplectic matrix:

$$\mathbf{J} = \begin{pmatrix} 0 & \mathbf{I} \\ -\mathbf{I} & 0 \end{pmatrix}, \tag{3}$$

where $\mathbf{I}$ is the identity matrix. The state space vector $\mathbf{V}$ can be defined by:

- for elastic solid media:

$$\mathbf{V} = [u_x, \quad u_y, \quad \sigma_{zz}, \quad \sigma_{xz}, \quad \sigma_{yz}, \quad u_z]^T, \tag{4}$$

- for poroelastic media:

$$\mathbf{V} = [u_x^s, \quad u_y^s, \quad \hat{\sigma}_{zz}^s, \quad -p, \quad \hat{\sigma}_{xz}^s, \quad \hat{\sigma}_{yz}^s, \quad u_z^s, \quad u_z^t]^T. \tag{5}$$

The state vector of a porous medium is composed of the components of the state vector of both the solid phase and the fluid phase. The solid phase is represented here by the *in-vacuo* skeleton: Solid phase displacements u_x^s, u_y^s, u_z^s and *in-vacuo* normal stresses $\hat{\sigma}_{xz}^s, \hat{\sigma}_{yz}^s, \hat{\sigma}_{zz}^s$. On the other hand, the fluid phase is represented by the normal total displacement u_z^t and the pressure p.

The matrix of operators $\mathbf{H}$ depends on the partial derivatives with respect to the in-plane direction (x, y), $\partial/\partial x$ and $\partial/\partial y$, on the frequency ω, and on the material parameters. Classically, the properties of the material used in engineering sciences are considered as constant in the volume, so that this matrix is a constant function of the variable z. Its expression of $\mathbf{H}$ can be found for orthotropic solid and poroelastic media in Appendices C.1 and C.2, respectively.

The general solution of Eq. (2) can be written under the form:

$$\mathbf{V}(\omega, x, y, z) = \mathbf{Z}(\omega, z - z_0)\mathbf{V}(\omega, x, y, z_0) \quad \text{for all } z, \tag{6}$$

where the matrizant $\mathbf{Z}$ can be computed by:

$$\mathbf{Z}(\omega, z) = \exp(-\mathbf{J}\mathbf{H}(\omega)z). \tag{7}$$

The equation of transfer Eq. (6) means that, once the state vector is known in one arbitrary section, it can be derived in all other sections at a very low numerical cost.

The matrix $\mathbf{H}$ depends on the partial derivatives of the state vector in the x and y directions. Consequently, the matrizant can only be computed by making an assumption on the variation of the state vector in the (x, y) plane, transverse to wave propagation. In practice, the elementary solutions are chosen in a basis of analytic functions of x and y, for example plane wave solutions, or are expressed as a Ritz superposition of sinusoidal or polynomial wave functions.[20] This assumption is the limit of this method, because depending on the BCs, no analytic expression for the fields may exist. Finally, the waves traveling in the material can be predicted by looking at the eigenmodes of the matrizant: The eigenvectors contain the shape of the waves, while the eigenvalues are called propagation constants and

are related to the wavenumbers k_{zi} and to the distance of propagation z by:

$$\lambda_i(z) = \exp(-jk_{zi}z), \tag{8}$$

where $j^2 = -1$.

2.2. *Transfer matrix method*

Among existing transfer matrix approaches, the TMM is a global transfer matrix method applied to the prediction of the vibroacoustic response of soundproofing packages. The method is thoroughly detailed by Allard and Atalla,[3] so only a brief review is provided here. This method is dedicated to structures of infinite lateral dimensions submitted to an acoustic pressure field in the (x, y) plane. The thickness is oriented in the z-direction. Plane waves and harmonic time are assumed: $\mathbf{V}(x, y, z, t) = \mathrm{Re}(\bar{\mathbf{V}}(z) \exp \times (j(\omega t - k_x x - k_y y)))$. The plate is excited by the air pressure, with the wavenumber $k_0 = \omega/c_0 = \sqrt{k_x^2 + k_y^2 + k_z^2}$. Elevation and azimuth angles θ and ϕ are defined by:

$$k_z = k_0 \cos\theta, \quad k_x = k_0 \sin\theta \cos\phi, \quad k_y = k_0 \sin\theta \sin\phi. \tag{9}$$

For isotropic material, the response of the structure is constant for all azimuth angles, so it is possible to simplify the three-dimensional representation to a two-dimensional view corresponding to the plane of incidence of the wave (Fig. 1). The transverse wavenumber k_t is thus defined by $k_t = k_0 \sin\theta$.

Unlike Stroh's formalism, the starting point of TMM is the analytic value of the wavenumbers and of the waveshapes. Knowing the value of the parameters of the material in the layer, these values can be obtained by making a Helmholtz decomposition of the solid and fluid displacements. In fluid media, there is one compression wave. In solid media, there are one longitudinal wave and one shear wave. In poroelastic media there are two longitudinal waves and one shear wave, due to the superposition of the fluid phase and of the solid phase. These waves propagate in both the solid phase and the fluid phase. The vector of the wavenumbers of the Helmholtz waves propagating in the medium is written in the following as $\mathbf{k} = (k_i)_{i\in\{1,2,3\}}$.

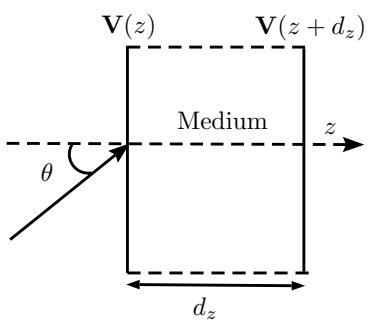

Fig. 1. Schema of TMM representation.

The transfer matrix $\mathbf{T}$ between two sections separated by a length d_z is expressed by using the decomposition of the state vector on the waves traveling through the material. First, all of the wavenumbers in the z-direction are written as:

$$k_{z,i} = \pm\sqrt{k_i^2 - k_t^2} \quad \text{for all wave } i. \tag{10}$$

Then the state vector is written as the sum of the contribution of each wave:

$$\bar{\mathbf{V}}(z) = \mathbf{G}(k_z, z, \omega)\mathbf{A}, \tag{11}$$

where $\mathbf{A}$ is the vector of the wave amplitudes in the layer and $\mathbf{G}$ is expressed analytically by using the expression of the wavenumbers and of the ratio between the amplitudes of the solid phase and the fluid phase for each propagative wave. Consequently, the state vectors at the two external sections are such as:

$$\bar{\mathbf{V}}(z + d_z) = \mathbf{G}(z + d_z)\mathbf{G}(z)^{-1}\bar{\mathbf{V}}(z) = \mathbf{T}(d_z)\bar{\mathbf{V}}(z). \tag{12}$$

Classically, it is said that the TMM is dedicated to the high frequency range, when the wavelengths are much shorter than the lateral dimensions. This statement is not exact, because it can be observed that the TMM is exactly equivalent to Stroh's formalism with a plane wave assumption: Indeed, in this case, wavenumbers and waveshapes used for the construction of $\mathbf{G}$ are exact. Consequently, the domain of validity of the TMM is not defined by a frequency range, but by the pertinence of the plane wave assumption depending on the problem.

2.3. *Finite element based TMM*

The WFE is a numerical TMM, based on the application of Floquet's theorem to a system of equations resulting from Finite Elements. The strength of the method is that using transfer propagators makes it possible to solve problems involving only as unknowns the degrees of freedom at both ends of the medium, compared to Finite Element Method in which all of the internal degrees of freedom are used as unknowns.

We consider here a three-dimensional waveguide of length L_z, composed of a single porous material, submitted in $z = L_z$ to a prescribed load $\mathbf{F}_{\text{imp}}$ and in $z = 0$ to a prescribed displacement $\mathbf{q}_{\text{imp}} = \mathbf{0}$. The approach is similar when two loads or two displacements are imposed on the two ends of the waveguide.

2.3.1. *Transfer matrix between two sections*

Because the section is assumed to be constant along the thickness, only a substructure of thickness d can be modeled. The equations of the dynamics discretized by FEM are written in the frequency domain under the form:

$$\mathbf{D}_f(\omega)\mathbf{q}_f = \mathbf{F}(\omega), \tag{13}$$

where $\mathbf{D}_f(\omega)$ is the dynamic stiffness matrix of the substructure, $\mathbf{q}_f$ is the vector of nodal unknowns and $\mathbf{F}$ is the vector of nodal loads.

Dirichlet conditions are applied in the dynamic stiffness matrix of the free substructure by multiplying it by a boolean matrix $\mathbf{\Gamma}$, and where $\mathbf{q}_r$ are the nonconstrained nodal degrees of freedom:

$$\mathbf{q}_f = \mathbf{\Gamma}\mathbf{q}_r, \quad \mathbf{D} = \mathbf{\Gamma}^T\mathbf{D}_f\mathbf{\Gamma}. \tag{14}$$

The resulting equations can be reorganized by separating the unknowns located on the left and right sections of the substructure, respectively L and R:

$$\begin{bmatrix} \mathbf{D}_{\mathrm{LL}} & \mathbf{D}_{\mathrm{LR}} \\ \mathbf{D}_{\mathrm{RL}} & \mathbf{D}_{\mathrm{RR}} \end{bmatrix} \begin{pmatrix} \mathbf{q}_{\mathrm{L}} \\ \mathbf{q}_{\mathrm{R}} \end{pmatrix} = \begin{pmatrix} \mathbf{F}_{\mathrm{L}} \\ \mathbf{F}_{\mathrm{R}} \end{pmatrix}, \tag{15}$$

where $\mathbf{q}$ and $\mathbf{F}$ are respectively the nodal displacements and the nodal loads.

Equation (15) can also be written in a transfer form:

$$\mathbf{T} \begin{pmatrix} \mathbf{q}_{\mathrm{L}} \\ -\mathbf{F}_{\mathrm{L}} \end{pmatrix} = \begin{pmatrix} \mathbf{q}_{\mathrm{R}} \\ \mathbf{F}_{\mathrm{R}} \end{pmatrix}, \tag{16}$$

where the transfer matrix $\mathbf{T}$ is given by:

$$\mathbf{T} = \begin{bmatrix} -\mathbf{D}_{\mathrm{LR}}^{-1}\mathbf{D}_{\mathrm{LL}} & -\mathbf{D}_{\mathrm{LR}}^{-1} \\ \mathbf{D}_{\mathrm{RL}} - \mathbf{D}_{\mathrm{RR}}\mathbf{D}_{\mathrm{LR}}^{-1}\mathbf{D}_{\mathrm{LL}} & -\mathbf{D}_{\mathrm{RR}}\mathbf{D}_{\mathrm{LR}}^{-1} \end{bmatrix}. \tag{17}$$

The state vector $[\mathbf{q}^T \quad \pm\mathbf{F}^T]^T$ is continuous between each layer of the same material, so the global transfer matrix can be written as a function of the number of elements $N = L_z/d$:

$$\begin{pmatrix} \mathbf{q} \\ \mathbf{F} \end{pmatrix}_{|z=L_z} = \mathbf{T}^N \begin{pmatrix} \mathbf{q} \\ -\mathbf{F} \end{pmatrix}_{|z=0} = \mathbf{\Phi}\mathbf{\Lambda}^N\mathbf{\Phi}^{-1} \begin{pmatrix} \mathbf{q} \\ -\mathbf{F} \end{pmatrix}_{|z=0}, \tag{18}$$

where $\mathbf{\Phi}$ is the matrix of eigenvectors of the transfer matrix $\mathbf{T}$ and $\mathbf{\Lambda}$ is the diagonal matrix of eigenvalues.

Because of the FE discretization in the section, the shape of the section modes takes into account the lateral BCs applied in the weak formulation and the Dirichlet BCs. Consequently, the dispersion curves also highlight the existence of BCs.

Applying this method directly may be possible in some cases, however it is subjected to several difficulties. First, the state vectors between two different materials are not continuous in the general case. For example, the fluid phase displacement is not necessarily continuous at the interface between two different poroelastic media. In this case, the total transfer matrix cannot be obtained directly by multiplying the transfer matrices of each layer. Second, numerical errors can occur during the inversion of the submatrix $\mathbf{D}_{\mathrm{LR}}$ and can be created if the substructure dimensions are too small or too large.[21] Third, the diagonal matrix of eigenvalues involves terms for incident waves $(+)$ $\exp(-jk_+z)$ and also for reflected waves $(-)$ $\exp(-jk_-z)$. The wavenumbers of incident and reflected waves are opposed: $k_+ = -k_-$, with $\mathrm{Re}(k_+) > 0$ and $\mathrm{Im}(k_+) < 0$. This means that in the direction $z > 0$, the amplitude of reflected waves increases exponentially. Moreover, the total number of waves is thus equal

to the size of the transfer matrix, i.e. to twice the number of degrees of freedom located in a section.

Small errors in one section are increased by the propagation in the medium with an exponential growth. The final solution can then be polluted by numerical errors. It has been shown[22] that this method is very efficient if only a few degrees of freedom are present in the section. However, it cannot be applied to reduce the number of degrees of freedom involved for poroelastic panels. Indeed, because of the small wavelengths traveling in such media, the section mesh has to be very refined, and the matrix of eigenvectors Φ is very large. Its inversion is both expensive in computational time and in memory. Furthermore, this method is not very stable, small numerical errors in one section being increased by the propagation of information in the medium with an exponential growth.

2.3.2. *Wave Finite Element Method*

The Wave Finite Element Method is an useful tool to compute dispersion properties in elastic media, either for 1D waveguides[12,13,23] or for bidirectional waveguides.[24,25] It can also be applied in the case of composites structures involving uncertainties,[26] different types of materials,[27,28] in particular poroelastic waveguides.[29] It can also be applied to compute the forced response of structures.[30–32] Floquet theorem states that on each section, state vector can be decomposed on a basis of modes Φ_i, which propagate with the constant λ_i. Such family of modes ($\mathbf{\Phi}, \mathbf{\Lambda} = \mathrm{diag}(\lambda)$) are the eigenmodes of the transfer matrix $\mathbf{T}$ (see Eq. (16)). Another way to compute these modes is proposed by Zhong[33] and is preferred in the literature dealing with WFE because it does not need to inverse the matrix $\mathbf{D}_{\mathrm{LR}}$. This approach has been used here. Finally, displacements and loads in each section of the whole structure are projected on the basis of propagative modes. The unknowns are the amplitudes of the incident and of the reflected waves:

$$\begin{pmatrix} \mathbf{q} \\ \pm\mathbf{F} \end{pmatrix}(z) = \begin{bmatrix} \mathbf{\Phi}_q^+ & \mathbf{\Phi}_q^- \\ \mathbf{\Phi}_F^+ & \mathbf{\Phi}_F^- \end{bmatrix} \begin{pmatrix} \mathbf{Q}^+ \\ \mathbf{Q}^- \end{pmatrix}(z), \tag{19}$$

where $Q^{\pm}$ is the vector of wave amplitudes and $\pm$ means the heading of the waves. Using Eq. (19) with Eq. (18) leads to an equation relating the amplitudes at two sections separated by a distance Nd with the diagonal matrix of eigenvalues, where N is the number of elements between the two sections and d the length of each element:

$$\begin{pmatrix} \mathbf{Q}^+ \\ \mathbf{Q}^- \end{pmatrix}(z + Nd) = \Lambda^N \begin{pmatrix} \mathbf{Q}^+ \\ \mathbf{Q}^- \end{pmatrix}(z). \tag{20}$$

To define if a wave is incident ($^+$) or reflected ($^-$), the variation of the wave amplitude from one section to another can be expressed:

$$\mathbf{Q}^+(z+d) = \mathbf{\Lambda}^+(d)\mathbf{Q}^+(z), \quad \mathbf{Q}^-(z+d) = \mathbf{\Lambda}^-(d)\mathbf{Q}^-(z), \tag{21}$$

with $\mathbf{\Lambda}^- = (\mathbf{\Lambda}^+)^{-1}$. In what follows, are considered as incident waves such as $|\lambda| \leq 1$ and reflected waves such as $|\lambda| > 1$. This means that $\|\mathbf{\Lambda}^+\| \leq 1$. If $\lambda = 1$, the distinction is made by writing that the work performed by the incident wave has to be negative, i.e.:

$$\mathrm{Re}(j\omega \mathbf{\Phi}_F \cdot \mathbf{\Phi}_q) < 0. \tag{22}$$

We note in the following $\mathbf{\Lambda} = \mathbf{\Lambda}^+$.

When forced response is considered, the main difficulty is to avoid propagation of numerical errors. The exponentially growing terms are only present in the reflected waves, more precisely in $\mathbf{\Lambda}^- = \mathrm{inv}(\mathbf{\Lambda})$. A good formulation should avoid to use such terms. Another source of numerical error is the different scales between the displacements $\mathbf{q}$ and the loads $\mathbf{F}$.

An approach has been proposed by Mencik[32] to solve for the problem with a good condition number. The unknowns are the amplitudes of the incident waves and of the reflected waves in one section, so BCs are needed on two sections, for example a given load $\mathbf{F}_{\mathrm{imp}}$ in $z = L_z$ and a prescribed displacement $\mathbf{q}_{\mathrm{imp}}$ in $z = 0$. In this case:

$$\begin{aligned} \mathbf{q}(0) = \mathbf{q}_{\mathrm{imp}} &= \mathbf{\Phi}_q^+ Q^+(0) + \mathbf{\Phi}_q^- Q^+(0), \\ \mathbf{F}(L_z) = \mathbf{F}_{\mathrm{imp}} &= \mathbf{\Phi}_F^+ Q^+(L_z) + \mathbf{\Phi}_F^- Q^+(L_z), \end{aligned} \tag{23}$$

so the amplitudes at the fluid excitation side verify:

$$\begin{bmatrix} \mathbf{I} & (\mathbf{\Phi}_F^-)^{-1}\mathbf{\Phi}_F^+\mathbf{\Lambda}^N \\ (\mathbf{\Phi}_q^+)^{-1}\mathbf{\Phi}_q^-\mathbf{\Lambda}^N & \mathbf{I} \end{bmatrix} \begin{bmatrix} \mathbf{I} & 0 \\ 0 & \mathbf{\Lambda}^{-N} \end{bmatrix} \begin{pmatrix} \mathbf{Q}^-(L) \\ \mathbf{Q}^+(L) \end{pmatrix} = \begin{pmatrix} (\mathbf{\Phi}_F^-)^{-1}\mathbf{F}_{\mathrm{imp}} \\ (\mathbf{\Phi}_q^+)^{-1}\mathbf{q}_{\mathrm{imp}} \end{pmatrix}. \tag{24}$$

After having solved for the amplitudes at the section L_z, the amplitudes are reconstructed section per section using Eq. (21), and displacements are reconstructed by using Eq. (19).

This formulation reduces numerical errors. Indeed, the scaling of the modes by premultiplying by inverse (terms $(\mathbf{\Phi}_q^+)^{-1}\mathbf{\Phi}_q^-$ and $(\mathbf{\Phi}_F^-)^{-1}\mathbf{\Phi}_F^+$) allows us to normalize loads and displacements to a similar value, and to reduce numerical influence of high order evanescent modes for which $|\lambda| \ll 1$.[32] Moreover, it can be observed with this formulation that BCs at the two extremities are verified in a strong sense.

The limit of this method is the numerical cost. To take into account the BCs, all of the modes, including evanescent ones, are needed. These evanescent modes may have complex shapes, so the mesh of the section should be fine enough to represent them correctly. However, it has been observed that these evanescent modes are important for representing clamped boundaries or geometric discontinuities, but have not so much influence on free displacements sections. The question of the optimal choice of a reduced basis of wave modes is always under investigation (see, e.g. Ref. 34), but it is not the object of the present paper.

When all of the waves are selected, the number of incident and reflected modes is equal to the number of unknowns located in one section for each of them. Large areas lead to a large number of degrees of freedom in the section, and so to huge memory to store all of

the eigenvectors and unaffordable time to invert the different matrices. However, for small number of degrees of freedom in section and for large propagation distances, the method leads to large reduction of computational times compared to direct finite element analysis (see, e.g. Refs. 12, 26 and 32). Another interesting aspect is that for this reason, WFE is not submitted to the usual FEM criterion saying that the mesh in the thickness has to be fine enough to represent well longitudinal modes of the solid phase and of the fluid phase. Usually when multilayers are considered, mesh refinement close to the interfaces is necessary. With WFE, only one element in the thickness is needed, resulting in possible reduction of computational times.

3. Effect of BCs on Wave Propagation

In this section, it is proposed to observe the influence of BCs on the waves propagating in the material and their consequences on acoustic indicators, for the three classes of poroelastic material: a very stiff one (material B), a very soft one (material C) and an intermediate material (material A). Their parameters are given in Table A.1. While the two phases are well decoupled in the second and the third materials, the first one exhibits strong coupling effects between the two phases, due to the rigidity rather small and resistivity rather large of the skeleton. The size of the section of the sample is $(L_x, L_y) = (10\,\text{cm} \times 8\,\text{cm})$ and its thickness is equal to $L_z = 5\,\text{cm}$ (Fig. 2). We consider propagation along z-axis. The face $z = 0$ is clamped and the sample is submitted to an uniform pressure field in $z = L_z$ (unitary pressure).

In a first section, the dispersion curves and absorption coefficient are compared depending on the lateral BCs (sliding or clamped), for three different materials. These BCs are

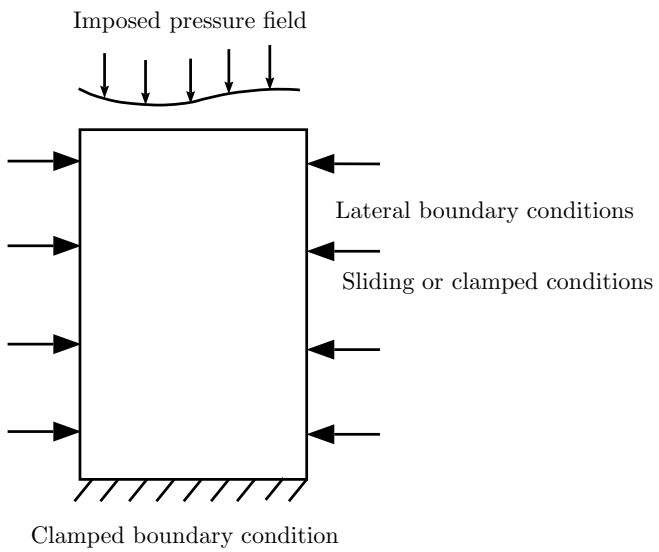

Fig. 2. Schema of the test case.

given in Eq. (25):

$$\begin{aligned} &\text{Sliding BC:}\ \ \mathbf{u}^s \cdot \mathbf{n} = 0 \text{ and } \mathbf{u}^t \cdot \mathbf{n} = 0 \text{ on the lateral walls,} \\ &\text{Clamped BC:}\ \ \mathbf{u}^s = \mathbf{0} \text{ and } \mathbf{u}^t \cdot \mathbf{n} = 0 \text{ on the lateral walls.} \end{aligned} \tag{25}$$

Unless written otherwise, the waves were calculated by using (10×8) H8 hexaedric linear elements in the section, and using for the size of the periodic substructure $d = 0.1$ mm, allowing us to make sure of the convergence of the results of the WFE on the entire frequency range. Finally, 10 elements were used in the thickness of the sample for FEM computations.

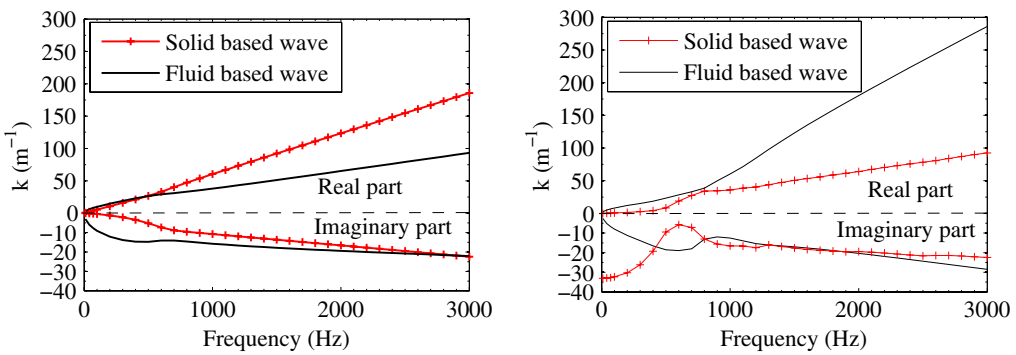

Fig. 3. Dispersion curves of zero-order propagative waves. (a) Sliding BC and (b) clamped BC.

3.1. *Case of a Biot's material (material A)*

The first propagative modes are the longitudinal waves (fluid and solid), so the discretization of the section has no effect on their dispersion curves. It can be seen in Fig. 3(a) that the sliding BC prevents the propagation of the first shear wave. The propagative waves are thus the two classical longitudinal waves, their waves shapes at 1000 Hz are presented in Fig. 4.

When clamped BCs are applied, the branch corresponding to longitudinal solid-based wave disappears (Fig. 3(b)). This means the clamped BC suppresses the longitudinal solid wave, propagative in low frequencies. However one longitudinal L_0 wave still exists, due to the presence of the fluid phase. Indeed, this wave is created by the interaction between the longitudinal wave of the air without skeleton, and of the first cross-section mode of the *in-vacuo* skeleton. When an acoustic plane wave impinges on the material, it makes the fluid phase move accordingly. The motion of the fluid phase generates thus a load on the solid phase, inducing thus a displacement of the solid phase similar to the one due to the first solid-based compression wave with clamped boundary. Due to the coupling, the motion of the solid phase modifies the displacement of the fluid phase as well.

The two waves traveling in the decoupled media are thus coupled in the poroelastic medium, so that the displacements of the fluid phase and of the solid phase are not uniform

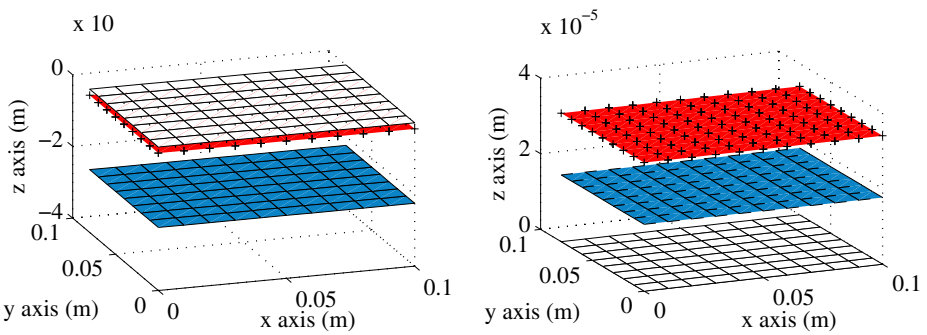

(a) (b)

Fig. 4. (Color online) Real part of mode shapes with sliding BC at 1000 Hz and material A (deformed and nondeformed configurations). Red, +: solid displacement; Blue, edge lines without markers: fluid displacement; white: nondeformed mesh. (a) Fluid based wave and (b) solid based wave.

in the section. It results in a propagative but dissipated mode, which can be called fluid based wave (see Fig. 6).

Furthermore, the first cross-section mode highlights also a coupling process between the two decoupled waves. When the first cross-section mode provided by the *in-vacuo* skeleton is excited, the fluid phase is also set in motion. It results in the same type of deformation as the fluid based propagative wave. This wave can be called solid based wave L_1, but is evanescent at low frequencies.

The existence of these two modes having similar shapes and similar wavenumbers is due to the strong couplings existing between the solid phase and the fluid phase. This happens because of the quite large resistivity value of the material. It can also be seen that these two modes couple between 500 Hz and 1000 Hz, with a veering effect at 800 Hz, so that above this critical frequency the fluid based wavenumber is larger than the solid based wavenumber. This coupling can be seen in the solid displacement of the fluid based mode shape (see Figs. 5(b) and 6(b)).

Finally, the wavenumbers obtained with sliding or clamped BCs are compared in Fig. 7(a) with those obtained for an infinite extent material. It can be observed that sliding BC and infinite extent BC result in the same dispersion curves. This means that longitudinal waves predicted with sliding BC have exactly the same behavior as Biot's waves for normal incidence excitation. This reflects the fact that sliding BC at normal incidence makes it possible to simulate for lateral infinite BCs. However, clamped BC modifies strongly the speed of this wave and its mode shape. This indicates that the coupling between the fluid phase and the solid phase is very strong.

It has been shown that for such material, the sliding and clamped BC result in different behaviors of waves. The influence of these different behaviors on the acoustic response of the sample can be seen in Fig. 7(b), where the absorption coefficients computed by WFE, FEM and TMM are plotted for the different BCs considered here.

A perfect agreement is observed for the absorption coefficient between FEM and WFE for both sliding and clamped BC. A classical stiffening effect is observed between 500 Hz

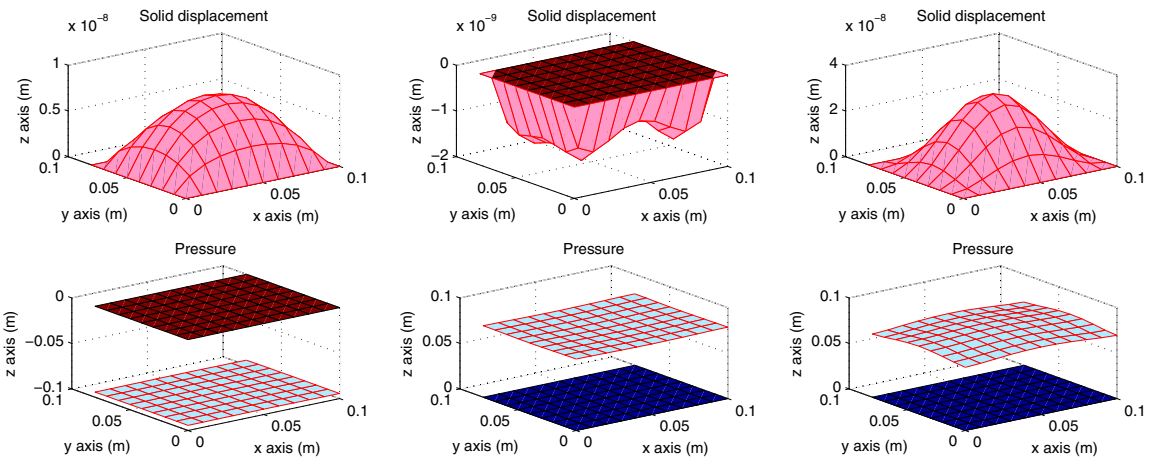

(a) (b) (c)

Fig. 5. Real part of mode shapes of L_0 wave with clamped BC. Top: Solid displacement, bottom: Pressure. (a) At 200 Hz, $k = (12.1 - 11.2j)\,\mathrm{m}^{-1}$, (b) At 600 Hz, $k = (28.5 - 18.9j)\,\mathrm{m}^{-1}$ and (c) At 800 Hz, $k = (38.8 - 13.1j)\,\mathrm{m}^{-1}$.

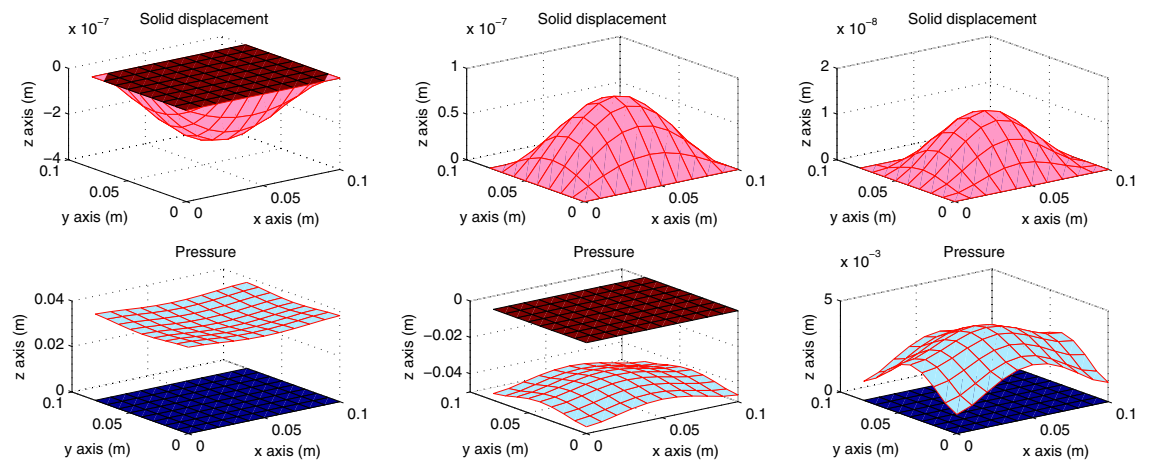

(a) (b) (c)

Fig. 6. Real part of mode shapes of L_1 wave with clamped BC. Top: Solid displacement, bottom: Pressure. (a) At 200 Hz, $k = (1.5 - 30.2j)\ \mathrm{m}^{-1}$, (b) At 600 Hz, $k = (19.0 - 5.9j)\ \mathrm{m}^{-1}$ and (c) At 800 Hz, $k = (34.0 - 13.1j)\ \mathrm{m}^{-1}$.

and 1000 Hz, clamped BC suppress the first resonance of the skeleton leading to a local minimum. This is due to the suppression of the propagative solid based wave. This effect leads also to a difference in the imaginary part of wavenumbers. The real part of Biot's slow wave however is quite the same as the smallest of the real part of L_0 and L_1 waves obtained with clamped BC. The frequency range of influence of BCs is the range in which neither of the L_0 and L_1 waves with clamped BC have the same wavenumber as the one obtained with sliding BC.

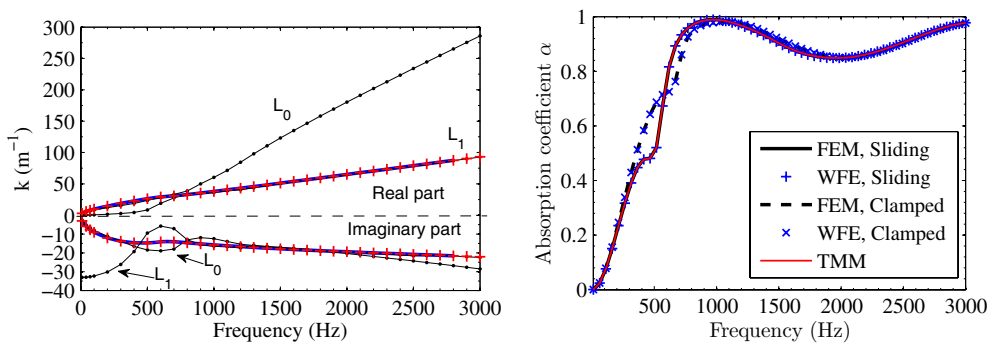

(a) (b)

Fig. 7. (Color online) Effects of BCs on a Biot's material (material A). (a) Dispersion curves for fluid based wave. Blue line: Analytic expression; red +: WFE Sliding; black line with dots: WFE Clamped L_0 and L_1. (b) Absorption coefficient at normal incidence.

More precisely, three domains can be separated. In the low frequency range, the wave L_0 is the fluid based propagative mode, it propagates with the same wavenumber with clamped or sliding BC, leading to the same absorption coefficient. The evanescent solid based wave is not much excited by the pressure excitation, and its influence is restricted to near field. Between 500 Hz and 1000 Hz the two modes L_0 and L_1 obtained with clamped BC couple together, exchanging energy, so that both the wavenumbers and the absorption coefficient are different from the case of sliding BC. This exchange of energy leads to a veering effect occurring at 800 Hz. At last, above 1000 Hz, the fluid based wave propagating with sliding BC have the same wavenumber than the wave L_1. It has been shown in Ref. 35 that the veering effect is associated to a change of behavior of the mode shape. The acoustic response for frequencies higher than the veering frequency is thus determined by the behavior of the wave L_1. It can be observed that this wave has the same wavenumber as the fluid based wave propagating with sliding BC, resulting in the same absorption coefficient.

TMM at normal incidence predicts correctly sliding BC only, because the longitudinal wave in this case is exactly the same as Biot's slow wave. Furthermore the shear wave is not excited at normal incidence because on one hand its amplitude is null so it has no contribution in TMM result, and on the other hand a propagative shear wave cannot even exist with sliding BC. Nonetheless, with clamped BC, the coupling between the shear wave and longitudinal deformation results in a nonplanar deformation.

3.2. *Case of a material with a high rigidity*

In this subsection, the same comparisons as previously are done, but a material with a large Young's modulus and a low resistivity is chosen (material B). Like for the elastic material, the rigid frame material exhibits two longitudinal waves with sliding BC, while only one is allowed by clamped CB. With sliding conditions the two longitudinal waves have uniform displacement in the section, while clamped condition results in a nonuniform

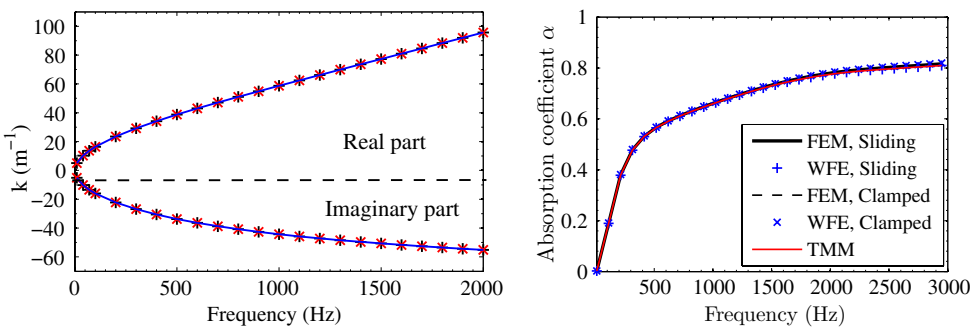

(a) (b)

Fig. 8. (Color online) Effects of BCs on a rigid material (material B). (a) Dispersion curves of the slow wave. Blue line: Analytic expression; black +: WFE, Sliding; red x: WFE Clamped. (b) Absorption coefficient at normal incidence.

shape, very similar to the one obtained with elastic material. For sake of conciseness, the mode shapes are not represented here, but it is worth noting that for this type of material, the amplitude of the fluid phase displacement is much larger than the amplitude of the solid phase displacement. The solid based wave which propagates with clamped BCs is not plotted here because it is purely evanescent in this range of frequency and does not couple with the fluid based propagative wave. Therefore, this mode does not have any influence on the acoustic response. This material can thus be modeled by using an equivalent fluid model (motionless skeleton).

Figure 8(a) presents the wavenumbers of the slow wave for the three BCs. The three curves are superposed, meaning the clamped BC has no effect on wave propagation in the sample. It was expected because for this material, the skeleton displacement is negligible in front of the fluid displacement. The absorption coefficients predicted by FEM, WFE and TMM are perfectly superposed for the two BCs (Fig. 8(b)).

In fact, the same behavior is observed between the two BCs because if the solid displacement is equal to zero, the work exerted by the lateral walls is also zero, as if infinite BCs had been considered. The dispersion curves in this configuration are presented in Fig. 9.

3.3. *Case of a material with a low rigidity*

In this section, the sample is made of material C. This material has a small Young's modulus, a Frame Stiffness Influence (FSI)[36] such as FSI ≤ 0.1, meaning the material can be modeled as an equivalent fluid with limp frame assumption. The difference with such material and the preceding ones is that because of the very low rigidity of the skeleton, waves propagate very slowly, i.e. with large wavenumbers and small wavelengths.

For such material, stresses exerted in the solid part are negligible in front of the fluid pressure, so the work of the lateral walls is equal to zero. Clamped and sliding BCs lead to similar results, except in the very low frequency range.

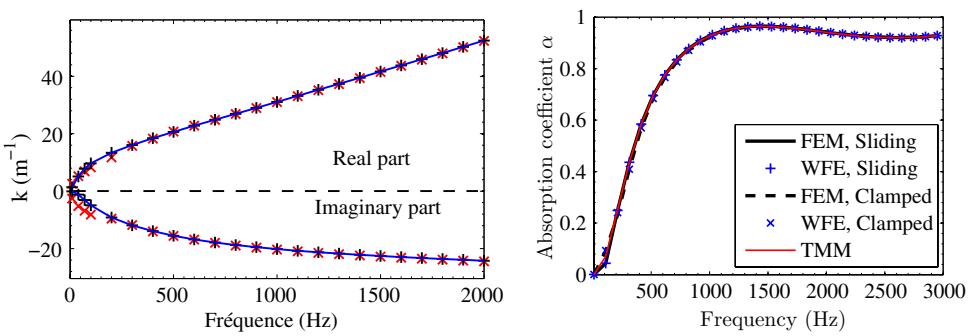

(a) (b)

Fig. 9. (Color online) Effects of BCs on a limp material (material C). (a) Dispersion curves of the slow wave. Blue line: Analytic expression; black +: WFE, Sliding; red x: WFE Clamped. (b) Absorption coefficient at normal incidence.

3.4. *Conclusion*

In this part was shown that in the general case TMM cannot take the BCs into account, due to the plane wave assumption. On the contrary, WFE makes it possible to predict the same results as Finite Elements for sliding or clamped BCs and for all kinds of materials.

TMM predicts correctly the normal impedance with sliding BC because the excitation is uniform on the section, the incidence is normal and sliding BC makes it possible to simulate in this case infinite BC. The behavior of the waves propagating in a infinite sample and in the finite size sample is thus identical. The only difference is that in the second case, no shear wave is allowed to propagate. The same behavior of the excited waves results then in a same absorption coefficient.

With clamped BC, the behavior of the propagating waves may be modified. For elastic material, strong coupling between the solid phase and the fluid phase results in different propagative waves, and so in different absorption coefficients. On the other hand, this is not the case for rigid and limp materials, due to the existence of a partial decoupling between the two phases. Thus, an equivalent fluid model would lead to a good prediction of the acoustic response of the sample, because the solid phase and the BCs have only a very small influence on the dispersion curves and on the response of the material.

In the next section, the acoustic response of the sample submitted to a nonuniform pressure field is observed.

4. Response of a Rigid Tube Filled with a Poroelastic Foam at Oblique Incidence

In this section, we consider the response of the same rigid tube filled with a poroelastic sample (material A, Table A.1), when sliding BC is applied and when a nonuniform pressure field is applied.

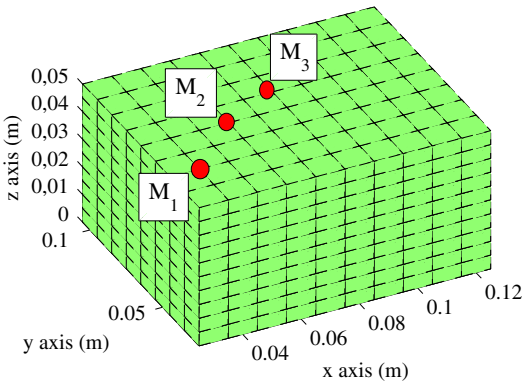

Fig. 10. (Color online) Mesh of the tube. Red dots: observation points.

4.1. *Oblique incidence*

First we consider an acoustic plane wave excitation impinging at a incidence $\theta = 45°$ and $\phi = 0°$ on surface $z = L_z$. The mesh used consists of 10×8 elements in the section, 10 elements in the thickness of the porous material (see Fig. 10). It has been verified that this mesh leads to a good convergence of the results up to 3 kHz.

Due to the oblique incidence, the response is nonuniform in the section. We define the nodal impedance at the point M of the interface by the ratio of the pressure and of the acoustic velocity at each node:

$$Z_s(M) = -\frac{p(M)}{\mathbf{v}(M) \cdot \mathbf{z}}. \tag{26}$$

Figure 11 presents the spectrum of the nodal impedance in the three points defined in Fig. 10: $M_1(2\text{ cm}, 1\text{ cm}), M_2(4\text{ cm}, 3\text{ cm}), M_1(5\text{ cm}, 5\text{ cm})$. A good superposition between FEM and WFE can be observed in the whole frequency range and at the three observation

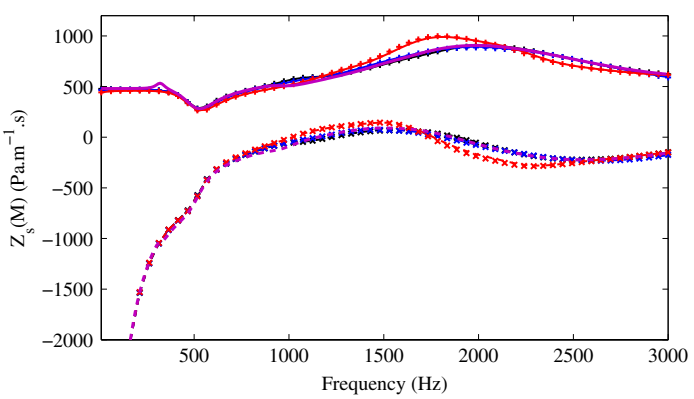

Fig. 11. (Color online) Nodal impedance on observation points. FEM: ▬ real part, ▪▪▪ imaginary part. WFE: + real part, **x** imaginary part. M_1: black, M_2: blue, M_3: red. TMM (incidence $\theta = 45°$): magenta.

points. The value of the impedance varies between the different points. It can be explained by the reflections of the waves on the lateral boundaries, leading to a nonlocal response. The value of the impedance predicted by TMM is thus an approximate value, which does not represent the complex behavior of the medium. This example highlights also the contradiction made by saying that TMM is a high frequency approach. Indeed, in the low frequency range, the material behaves as a locally reacting material, so TMM leads to good results. On the contrary, in higher frequencies, the reaction is nonlocal because several reflections on the lateral boundaries may occur. The acoustic response of the sample is not uniform on the section, and so TMM is not able to capture this spatial dependency.

4.2. *Modal field excitation*

In the high frequency range, several waves which were evanescent in the lower frequency range are able to propagate in an acoustic tube. If the tube has a rectangular section, an acoustic section mode can be written as:

$$p_e(x,y) = \cos(px)\cos(qy), \tag{27}$$

with $p = m\pi/L_x$ and $q = n\pi/L_y$. Because of the continuity of the pressure, it is assumed that the state vector in the poroelastic sample can be written on a sine and cosine basis:

$$\begin{aligned}
u_x^s(x,y,z) &= U_x(z)\sin(px)\cos(qy),\\
u_y^s(x,y,z) &= U_y(z)\cos(px)\sin(qy),\\
\hat{\sigma}_{zz}^s(x,y,z) &= \Sigma_{zz}(z)\cos(px)\cos(qy),\\
p(x,y,z) &= P(z)\cos(px)\cos(qy),\\
\hat{\sigma}_{xz}^s(x,y,z) &= \Sigma_{xz}(z)\sin(px)\cos(qy),\\
\hat{\sigma}_{yz}^s(x,y,z) &= \Sigma_{yz}(z)\cos(px)\sin(qy),\\
u_z^s(x,y,z) &= U_z(z)\cos(px)\cos(qy),\\
u_z^t(x,y,z) &= U_z^t(z)\cos(px)\cos(qy).
\end{aligned} \tag{28}$$

Then, using this approximation together with Eq. (2) allows the analytic expression of the transfer matrix $\mathbf{T}_{mn}$ between the two external sections $z = 0$ and $z = L_z$ to be derived. The BCs can be expressed as follows:

- at $z = 0$: $U_x(0) = U_y(0) = U_z(0) = U_z^t(0) = 0$;
- at $z = L_z$: $P(L_z) = 1,\ \Sigma_{xz}(L_z) = \Sigma_{yz}(L_z) = \Sigma_{zz}(L_z) = 0$.

Combining the BCs and the transfer matrix makes it possible to compute first the state vectors at the two ends of the sample, then to derive the displacement and the stress fields in the whole poroelastic domain. Finally, the value of the surface impedance in $z = L_z$ can be obtained.

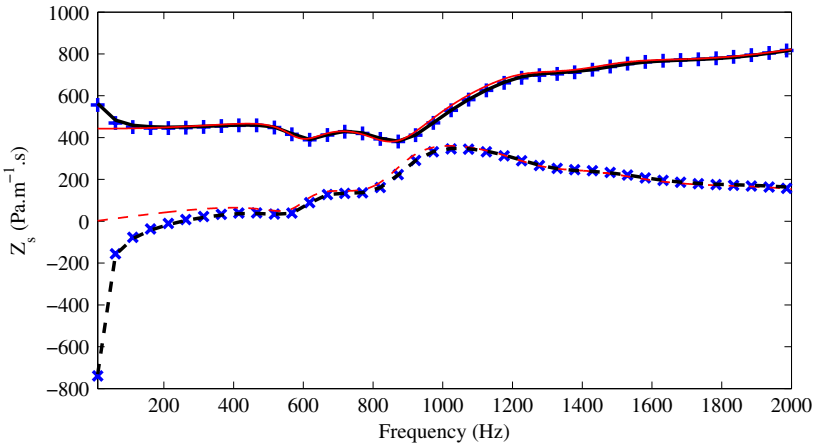

Fig. 12. (Color online) Surface impedance of the sample. FEM (black): ▬ Real part, ▪ ▪ ▪ Imaginary part. WFE (blue): + Real part, x Imaginary part. Analytic (red): —— Real part, – – – Imaginary part.

In the present case, we consider the mode $(m = 1, n = 1)$. Figure 12 presents the nodal impedance of the observation points computed by FEM, WFE, with the impedance predicted by the analytic method (Stroh's formalism with a field satisfying Eqs. (28), or TMM with $k_x = \pi/L_x$ and $k_y = \pi/L_y$).

A perfect superposition between FEM and WFE can again be observed on the whole frequency range, for each of the three observation points. The value of the impedance predicted by TMM is different, because a nonlocal behavior is forced. The cross-section modes traveling in the poroelastic medium are excited by this nonuniform excitation, so that the response cannot be predicted accurately by taking into account only the propagative waves, like it is done in TMM. Finally, the analytic approach makes it possible to predict accurately the nodal impedance, for frequency above 500 Hz. Indeed, for lower frequencies, the mode $(1, 1)$ is not propagative in the sample. Consequently, if the field can be expressed as Eq. (28) at $z = L_z$, this approximation is no longer valid for other sections $z \in [0, L_z]$. This explains the difference between the impedance computed by FEM and the value predicted by the analytic approach. To sum up, this example shows that analytic approaches, TMM or Stroh's formalism, allow the response of the material to be to predicted, but only when the assumptions on the waveshape in the material are valid. In the low frequency range, these shapes may not be pertinent because of the existence of the lateral BCs and because such modes are evanescent and do not propagate in the whole thickness in the sample. These limitations can be overcome by using a numerical approach like WFE.

5. Conclusion

An investigation of the relationships between three TMMs has been presented and how these methods can take into account the lateral BCs. It is explicitly shown by observing the effects of different BCs on wave propagation and acoustic response of a reduced size sample

that wave approaches cover from the low frequency range to the high frequency range. Thus, WFE leads to the same results than Finite Elements, but needs only one element in the thickness. This method is dedicated to the low frequency range, due to the low frequency restriction of Finite Elements. It stays valid for higher frequencies, at a larger numerical cost. On the other hand, analytic methods such as TMM are limited not in the frequency band considered but in the analytic assumption concerning the shape of the modes in the section and the value of the wavenumbers. The pertinence of such assumptions depends on both the material and the geometry. Consequently, TMM applies well to geometries in which only plane waves travel in the material. It is often the case in the high frequency range for geometries involving large section areas. It is also the case for poroelastic materials with very soft or stiff skeletons, even in presence of lateral BCs.

Acknowledgments

The research presented in this paper was performed within the framework of the LABEX CELYA ("Centre Lyonnais d'Acoustique", ANR-10-LABX-0060) of Université de Lyon, and funded by a doctoral grant of the French Ministry of Higher Education and Research.

References

1. W. T. Thomson, Transmission of elastic waves through a stratified solid medium, *J. Appl. Phys.* **21**(2) (1950) 89–93.
2. N. A. Haskell, The dispersion of surface waves on multilayered media, *Bull. Seismol. Soc. Am.* **43**(1) (1953) 17–34.
3. J.-F. Allard and N. Atalla, *Propagation of Sound in Porous Media: Modelling Sound Absorbing Materials*, 2nd edn. (Wiley, New York, 2009).
4. B. Brouard, D. Lafarge and J.-F. Allard, A general method of modelling sound propagation in layered media, *J. Sound Vibr.* **183**(1) (1995) 129–142.
5. N. Atalla, R. Panneton and P. Debergue, A mixed displacement-pressure Formulation for poroelastic materials, *J. Acoust. Soc. Am.* **104**(3) (1998) 1444–1452.
6. P. Göransson, A 3-D, symmetric, finite element formulation of the Biot equations with application to acoustic wave propagation through an elastic porous medium, *Int. J. Numer. Methods Eng.* **41**(1) (1998) 167–192.
7. F. Chevillotte and R. Panneton, Coupling transfer matrix method to finite element method for analyzing the acoustics of complex hollow body networks, *Appl. Acoust.* **72**(12) (2011) 962–968.
8. L. Alimonti, N. Atalla, A. Berry and F. Sgard, A hybrid modeling approach for vibroacoustic systems with attached sound packages, in *Proc. Meetings on Acoustics*, Vol. 19, 7 June 2013, Montréal, Canada, 2013, pp. 1–9.
9. A. Dijckmans and G. Vermeir, Development of a hybrid wave based–transfer matrix model for sound transmission analysis, *J. Acoust. Soc. Am.* **133**(4) (2013) 2157–2168.
10. M. Villot, C. Guigou and L. Gagliardini, Predicting the acoustical radiation of finite size multilayered structures by applying spatial windowing on infinite structures, *J. Sound Vibr.* **245**(3) (2001) 433–455.
11. D. Rhazi and N. Atalla, A simple method to account for size effects in the transfer matrix method, *J. Acoust. Soc. Am.* **127**(2) (2010) 30–36.
12. J.-M. Mencik and M. N. Ichchou, Multi-mode propagation and diffusion in structures through finite elements, *Eur. J. Mech. A. Solids* **24**(5) (2005) 877–898.

13. B. R. Mace, D. Duhamel, M. J. Brennan and L. Hinke, Finite element prediction of wave motion in structural waveguides, *J. Acoust. Soc. Am.* **117**(5) (2005) 2835–2843.
14. Y. J. Kang and J. S. Bolton, Finite element modeling of isotropic elastic porous materials coupled with acoustical finite elements, *J. Acoust. Soc. Am.* **98**(1) (1995) 635–643.
15. B. H. Song, J. S. Bolton and Y. J. Kang, Effect of circumferential edge constraint on the acoustical properties of glass fiber materials, *J. Acoust. Soc. Am.* **110**(6) (2001) 2902–2916.
16. H. Aygun and K. Attenborough, Sound absorption by clamped poroelastic plates, *J. Acoust. Soc. Am.* **124**(3) (2008) 1550–1556.
17. M. A. Biot, Mechanics of deformation and acoustic propagation in porous media, *J. Appl. Phys.* **33**(4) (1962) 1482–1498.
18. N. Atalla, M. A. Hamdi and R. Panneton, Enhanced weak integral formulation for the mixed (u, p) poroelastic equations, *J. Acoust. Soc. Am.* **109**(6) (2001) 3065–3068.
19. O. Dazel, B. Brouard, C. Depollier and S. Griffiths, An alternative Biot's displacement formulation for porous materials, *J. Acoust. Soc. Am.* **121**(6) (2007) 3509–3516.
20. A. Benjeddou and J.-F. Deü, Piezoelectric transverse shear actuation and sensing of plates, Part 1: A three-dimensional mixed state space formulation, *J. Intell. Mater. Syst. Struct.* **12**(7) (2001) 435–449.
21. D. Duhamel, B. R. Mace and M. J. Brennan, Finite element analysis of the vibrations of waveguides and periodic structures, *J. Sound Vibr.* **294**(1) (2006) 205–220.
22. G. Gosse, C. Pézerat and F. Bessac, Vibroacoustique d'une structure périodique de type batterie à ailettes, in *Actes du 10ème Congrès Francais d'Acoustique* (SFA Paris, Lyon, France, 2010), pp. 1–5.
23. L. Houillon, M. N. Ichchou and L. Jezequel, Wave motion in thin-walled structures, *J. Sound Vibr.* **281**(3) (2005) 483–507.
24. B. R. Mace and E. Manconi, Modelling wave propagation in two-dimensional structures using finite element analysis, *J. Sound Vibr.* **318**(4) (2008) 884–902.
25. E. Manconi and S. Sorokin, On the effect of damping on dispersion curves in plates, *Int. J. Solids Struct.* **50**(11–12) (2013) 1966–1973.
26. M. A. Ben Souf, O. Bareille, M. N. Ichchou, F. Bouchoucha and M. Haddar, Waves and energy in random elastic guided media through the stochastic wave finite element method, *Phys. Lett. A* **377**(37) (2013) 2255–2264.
27. D. Chronopoulos, B. Troclet, O. Bareille and M. N. Ichchou, Modeling the response of composite panels by a dynamic stiffness approach, *Compos. Struct.* **96** (2013) 111–120.
28. C. Droz, J.-P. Lainé, M. N. Ichchou and G. Inquiété, A reduced formulation for the free-wave propagation analysis in composite structures, *Compos. Struct.* **113** (2013) 134–144.
29. Q. Serra, M. N. Ichchou and J.-F. Deü, Wave properties in poroelastic media using a wave finite element method, *J. Sound Vibr.* **335** (2015) 125–146.
30. Y. Waki, B. R. Mace and M. J. Brennan, Free and forced vibrations of a tyre using a wave/finite element approach, *J. Sound Vibr.* **323**(3) (2009) 737–756.
31. J. M. Renno and B. R. Mace, On the forced response of waveguides using the wave and finite element method, *J. Sound Vibr.* **329**(26) (2010) 5474–5488.
32. J.-M. Mencik, On the low-and mid-frequency forced response of elastic structures using wave finite elements with one-dimensional propagation, *Comput. Struct.* **88**(11) (2010) 674–689.
33. W. X. Zhong and F. W. Williams, On the direct solution of wave propagation for repetitive structures, *J. Sound Vibr.* **181**(3) (1995) 485–501.
34. J.-M. Mencik, A model reduction strategy for computing the forced response of elastic waveguides using the wave finite element method, *Comput. Methods Appl. Mech. Eng.* **229** (2012) 68–86.

35. B. R. Mace and E. Manconi, Wave motion and dispersion phenomena: Veering, locking and strong coupling effects, *J. Acoust. Soc. Am.* **131**(2) (2012) 1015–1028.
36. O. Doutres, N. Dauchez, J.-M. Génevaux and O. Dazel, Validity of the limp model for porous materials: A criterion based on the Biot theory, *J. Acoust. Soc. Am.* **122**(4) (2007) 2038–2048.
37. D. L. Johnson, J. Koplik and R. Dashen, Theory of dynamic permeability and tortuosity in fluid-saturated porous media, *J. Fluid Mech.* **176**(1) (1987) 379–402.
38. Y. Champoux and J.-F. Allard, Dynamic tortuosity and bulk modulus in air-saturated porous media, *J. Appl. Phys.* **70**(4) (1991) 1975–1979.
39. D. Rhazi and N. Atalla, Transfer matrix modeling of the vibroacoustic response of multi-materials structures under mechanical excitation, *J. Sound Vibr.* **329**(13) (2010) 2532–2546.
40. M. A. Biot and D. G. Willis, The elastic coefficients of the theory of consolidation, *J. Appl. Mech.* **24** (1957) 594–601.

Appendix A: Material Parameters

In the Biot–Allard theory, using Johnson's approximation[37] for the effective density and Champoux–Allard approximation[38] for the equivalent bulk modulus, nine coefficients are needed to describe the vibroacoustic response of a poroelastic materials. Parameters of the materials used in the present paper are given in Table A.1.

Appendix B: Biot–Allard Theory

All of the details concerning the following expressions can be found in Refs. 3, 19 and 40. The following expressions are obtained with a time-harmonic dependency $\exp(j\omega t)$. We consider here the Johnson–Champoux–Allard model for the expression of the material parameters.

Table A.1. Parameters of the materials.

Parameter	Material A[39]	Material B[4]	Material C[36]
Acoustic parameters			
Porosity ϕ	0.98	0.99	0.95
Resistivity σ ($\mathrm{N \cdot s \cdot m^{-4}}$)	22 000	10 000	23 000
Tortuosity α_∞	1.9	1.0	1
Viscous length Λ (μm)	87	120	54.1
Thermal length Λ' (μm)	146	120	162.3
Structural parameters			
Skeleton density ρ_s ($\mathrm{kg \cdot m^{-3}}$)	30	100	58
First Lame's coefficient λ (Pa)	80 556	0	0
Second Lame's coefficient μ (Pa)	120 830	50×10^6	8500
Hysteretic dissipation η	0.18	0.02	0.1
Ambient fluid parameters			
Ambient fluid density ρ_0 ($\mathrm{kg \cdot m^{-3}}$)		1.21	
Ambient fluid dynamic viscosity η_f ($10^{-5}\mathrm{N \cdot m^{-1} \cdot s^{-1}}$)		1.84	
Standard pressure P_0 (Pa)		101 325	
Heat capacity ratio γ		1.4	
Prandtl's number (Pr)		0.71	

B.1. *Inertial coefficients*

The equivalent densities $\tilde{\rho}_{11}$, $\tilde{\rho}_{22}$, $\tilde{\rho}_{12}$ are related to the density of the *in-vacuo* skeleton ρ_s and to the density of the fluid ρ_0 by:

$$\tilde{\rho}_{12} = -\phi\rho_0(\alpha_\infty - 1) + \frac{j\tilde{b}}{\omega}, \quad \tilde{\rho}_{11} = \rho_s - \tilde{\rho}_{12}, \quad \tilde{\rho}_{22} = \phi\rho_0 - \tilde{\rho}_{12}, \tag{B.1}$$

where the viscous correction function $\tilde{b}(\omega)$ is given by Johnson's model:

$$\tilde{b} = \sigma\phi^2 \left(1 + \frac{4j\omega\eta_f\alpha_\infty^2\rho_0}{(\sigma\lambda\phi)^2}\right)^{1/2}. \tag{B.2}$$

The equivalent densities $\tilde{\rho}$, $\tilde{\rho}_s$ and $\tilde{\rho}_{\text{eq}}$ are given by:

$$\tilde{\rho} = \tilde{\rho}_{11} - \frac{\tilde{\rho}_{12}^2}{\tilde{\rho}_{22}}, \quad \tilde{\rho}_s = \tilde{\rho} + \tilde{\gamma}^2\rho_{\text{eq}}, \quad \tilde{\rho}_{\text{eq}} = \frac{\rho_{22}}{\phi^2}, \tag{B.3}$$

where the coupling coefficient $\tilde{\gamma}$ is given by:

$$\tilde{\gamma} = \phi\left(\frac{\tilde{\rho}_{12}}{\tilde{\rho}_{22}} - \frac{1-\phi}{\phi}\right). \tag{B.4}$$

B.2. *Elastic coefficients*

The elastic coefficients are given by using the stress–strain relations of the elastic *in-vacuo* skeleton:

$$\hat{\boldsymbol{\sigma}}^{\boldsymbol{s}} = \hat{\mathbf{C}} : \frac{\boldsymbol{\nabla}\mathbf{u}^s + \boldsymbol{\nabla}^T\mathbf{u}^s}{2}. \tag{B.5}$$

The fluid bulk modulus is given by Champoux–Allard's model:

$$\tilde{K}_f = \frac{\gamma P_0}{\gamma - (\gamma-1)\left[1 + \dfrac{8\eta_f}{j\omega P_r\Lambda'^2\rho_0}\left(1 + \dfrac{j\omega P_r\Lambda'^2\rho_0}{16\eta_f}\right)^{1/2}\right]^{-1}}. \tag{B.6}$$

Finally, the bulk modulus of the equivalent fluid with motionless skeleton is:

$$\tilde{K}_{\text{eq}} = \frac{\tilde{K}_f}{\phi}, \tag{B.7}$$

B.3. *Dynamic equilibrium*

Finally, with $(\mathbf{u}^s, \mathbf{u}^t)$ formulation, the dynamic equilibrium is given by:

$$\boldsymbol{\nabla}\cdot\hat{\boldsymbol{\sigma}}^{\boldsymbol{s}} = -\omega^2\tilde{\rho}_s\mathbf{u}^s - \omega^2\tilde{\gamma}\tilde{\rho}_{\text{eq}}\mathbf{u}^t, \tag{B.8a}$$

$$-\boldsymbol{\nabla}p = -\omega^2\tilde{\gamma}\tilde{\rho}_{\text{eq}}\mathbf{u}^s - \omega^2\tilde{\rho}_{\text{eq}}\mathbf{u}^t, \tag{B.8b}$$

$$\hat{\boldsymbol{\sigma}}^{\boldsymbol{s}} = \frac{1}{2}\hat{\mathbf{C}} : (\boldsymbol{\nabla}\mathbf{u}^s + \boldsymbol{\nabla}^T\mathbf{u}^s), \tag{B.8c}$$

$$p = -\tilde{K}_{\text{eq}}\boldsymbol{\nabla}\cdot\mathbf{u}^t, \tag{B.8d}$$

where $\mathbf{u}^s = (u_x^s, u_y^s, u_z^s)^T$ and $\mathbf{u}^t = (u_x^t, u_y^t, u_z^t)^T$ are respectively the vector of the three solid displacements and the vector of the three total displacements.

Appendix C. Transfer Matrices in the Thickness of a Plate

We consider here an orthotropic flat panel lying in the (x, y)-plane, the thickness being directed in the z-axis. The matrix $\mathbf{H}$ used in Eq. (2) can be expressed as:

$$\mathbf{H} = \begin{bmatrix} \mathbf{H}_1 & 0 \\ 0 & \mathbf{H}_2 \end{bmatrix}, \tag{C.1}$$

where $\mathbf{H}_1$ and $\mathbf{H}_2$ are given in the following subsections depending on the type of the material.

C.1. *Solid layer*

The displacement is written $\mathbf{u} = u_x\mathbf{x} + u_y\mathbf{y} + u_z\mathbf{z}$. The stress–strain relation is expressed in the general way for an orthotropic medium:

$$\begin{pmatrix} \sigma_{xx} \\ \sigma_{yy} \\ \sigma_{zz} \\ \sigma_{yz} \\ \sigma_{xz} \\ \sigma_{xy} \end{pmatrix} = \begin{bmatrix} C_{11} & C_{12} & C_{13} & 0 & 0 & 0 \\ C_{12} & C_{22} & C_{23} & 0 & 0 & 0 \\ C_{13} & C_{23} & C_{33} & 0 & 0 & 0 \\ 0 & 0 & 0 & C_{44} & 0 & 0 \\ 0 & 0 & 0 & 0 & C_{55} & 0 \\ 0 & 0 & 0 & 0 & 0 & C_{66} \end{bmatrix} \begin{pmatrix} \epsilon_{xx} \\ \epsilon_{yy} \\ \epsilon_{zz} \\ 2\epsilon_{yz} \\ 2\epsilon_{xz} \\ 2\epsilon_{xy} \end{pmatrix}, \tag{C.2}$$

where $\epsilon_{ij} = \frac{1}{2}(\frac{\partial u_i}{\partial j} + \frac{\partial u_j}{\partial i})$ for $(i, j) \in \{x, y, z\}^2$.

The state vector is given by:

$$\mathbf{V} = [u_x, \quad u_y, \quad \sigma_{zz}, \quad \sigma_{xz}, \quad \sigma_{xz}, \quad u_z]^T. \tag{C.3}$$

The matrices $\mathbf{H}_1$ and $\mathbf{H}_2$ can be written as:

$$\mathbf{H}_1 = \begin{bmatrix} -\rho\omega^2 - C'_{11}\dfrac{\partial^2}{\partial x^2} - C_{66}\dfrac{\partial^2}{\partial y^2} & -(C'_{12} + C_{66})\dfrac{\partial^2}{\partial x \partial y} & -\dfrac{C_{13}}{C_{33}}\dfrac{\partial}{\partial x} \\ -(C'_{12} + C_{66})\dfrac{\partial^2}{\partial x \partial y} & -\rho\omega^2 - C'_{22}\dfrac{\partial^2}{\partial y^2} - C_{66}\dfrac{\partial^2}{\partial x^2} & -\dfrac{C_{23}}{C_{33}}\dfrac{\partial}{\partial y} \\ -\dfrac{C_{13}}{C_{33}}\dfrac{\partial}{\partial x} & -\dfrac{C_{23}}{C_{33}}\dfrac{\partial}{\partial y} & \dfrac{1}{C_{33}} \end{bmatrix} \tag{C.4}$$

and

$$\mathbf{H}_2 = \begin{bmatrix} -\dfrac{1}{C_{55}} & 0 & \dfrac{\partial}{\partial x} \\ 0 & -\dfrac{1}{C_{44}} & \dfrac{\partial}{\partial y} \\ \dfrac{\partial}{\partial x} & \dfrac{\partial}{\partial y} & \rho\omega^2 \end{bmatrix}, \tag{C.5}$$

where $C'_{11} = C_{11} - C_{13}^2/C_{33}$, $C'_{22} = C_{22} - C_{23}^2/C_{33}$ and $C'_{12} = C_{12} - C_{13}C_{23}/C_{33}$.

C.2. *Poroelastic layer*

Porous material is modeled using Biot–Allard's theory (see Appendix 5). The state vector is expressed as:

$$\mathbf{V} = [u_x^s, \quad u_y^s, \quad \hat{\sigma}_{zz}^s, \quad -p, \quad \hat{\sigma}_{xz}^s, \quad \hat{\sigma}_{yz}^s, \quad u_z^s, \quad u_z^t]^T. \tag{C.6}$$

The tensor of elastic coefficients of the *in-vacuo* skeleton is written $\hat{\mathbf{C}}$ and is expressed in the same way as for an elastic solid Eq. (C.2). The matrices $\mathbf{H}_1$ and $\mathbf{H}_2$ are thus defined by:

$$\mathbf{H}_1 = \begin{bmatrix} \Gamma_1 & -(\hat{C}'_{12} + \hat{C}_{66})\dfrac{\partial^2}{\partial x \partial y} & -\dfrac{\hat{C}_{13}}{\hat{C}_{33}}\dfrac{\partial}{\partial x} & \tilde{\gamma}\dfrac{\partial}{\partial x} \\ -(\hat{C}'_{12} + \hat{C}_{66})\dfrac{\partial^2}{\partial x \partial y} & \Gamma_2 & -\dfrac{\hat{C}_{23}}{\hat{C}_{33}}\dfrac{\partial}{\partial y} & \tilde{\gamma}\dfrac{\partial}{\partial y} \\ -\dfrac{\hat{C}_{13}}{\hat{C}_{33}}\dfrac{\partial}{\partial x} & -\dfrac{\hat{C}_{23}}{\hat{C}_{33}}\dfrac{\partial}{\partial y} & \dfrac{1}{\hat{C}_{33}} & 0 \\ \tilde{\gamma}\dfrac{\partial}{\partial x} & \tilde{\gamma}\dfrac{\partial}{\partial y} & 0 & \Gamma_3 \end{bmatrix} \tag{C.7}$$

and

$$\mathbf{H}_2 = \begin{bmatrix} -\dfrac{1}{\hat{C}_{55}} & 0 & \dfrac{\partial}{\partial x} & 0 \\ 0 & -\dfrac{1}{\hat{C}_{44}} & \dfrac{\partial}{\partial y} & 0 \\ \dfrac{\partial}{\partial x} & \dfrac{\partial}{\partial y} & \tilde{\rho}_s\omega^2 & \tilde{\rho}_{\mathrm{eq}}\tilde{\gamma}\omega^2 \\ 0 & 0 & \tilde{\rho}_{eq}\tilde{\gamma}\omega^2 & \tilde{\rho}_{\mathrm{eq}}\omega^2 \end{bmatrix}, \tag{C.8}$$

where $\hat{C}'_{11} = \hat{C}_{11} - \hat{C}^2_{13}/\hat{C}_{33}$, $\hat{C}'_{22} = \hat{C}_{22} - \hat{C}^2_{23}/\hat{C}_{33}$ and $\hat{C}'_{12} = \hat{C}_{12} - \hat{C}_{13}\hat{C}_{23}/\hat{C}_{33}$, and where:

$$\begin{aligned}
\Gamma_1 &= -\omega^2\tilde{\rho} - \hat{C}'_{11}\frac{\partial^2}{\partial x^2} - \hat{C}_{66}\frac{\partial^2}{\partial y^2}, \\
\Gamma_2 &= -\omega^2\tilde{\rho} - \hat{C}'_{22}\frac{\partial^2}{\partial y^2} - \hat{C}_{66}\frac{\partial^2}{\partial x^2}, \\
\Gamma_3 &= \frac{1}{\tilde{K}_{\mathrm{eq}}} + \frac{1}{\tilde{\rho}_{\mathrm{eq}}\omega^2}\left(\frac{\partial^2}{\partial x^2} + \frac{\partial^2}{\partial y^2}\right).
\end{aligned} \tag{C.9}$$